

Tracking flow: Decoding dynamic flow experience on a sub-minute timescale through performance in fine fingertip force control task

Bohao Tian^a, Shijun Zhang^a, Sirui Chen^a, Yuru Zhang^a, Kaiping Peng^b, Hongxing Zhang^c and Dangxiao Wang^{ad*}

^aState Key Laboratory of Virtual Reality Technology and Systems, Beihang University, Beijing, 100191, People's Republic of China

^bDepartment of Psychology, Tsinghua University, Beijing, 100084, People's Republic of China

^cState Key Laboratory of Proteomics, Beijing, 102206, People's Republic of China

^dPeng Cheng Laboratory, Shenzhen, 518000, People's Republic of China

Corresponding author: *Dangxiao Wang

Email: hapticwang@buaa.edu.cn

Abstract

Flow, an optimal mental state merging action and awareness, significantly impacts performance, emotion and wellbeing in real-world contexts. However, capturing its fluctuations on a sub-minute timescale is challenging due to the sparsity of the existing flow measuring tools. Here we present a virtual reality fine fingertip force control (F³C) task to induce flow, wherein the task challenge is set at a compatible level with personal skill, and to track the flow fluctuations from the synchronous force control performance. We extract eight performance metrics from the fingertip force sequence and reveal their significant differences under distinct flow states. Further, we built a flow decoder and demonstrated that the flow variations can be decoded using selected metrics. The predicted values reach significant correlation with the self-reported flow intensity ($r=0.81$). This study showcases the feasibility of tracking intrinsic flow variations with high temporal resolution using task performance measures.

Keywords: Flow experience; fine fingertip force control; task performance; sub-minute timescale; dynamics

1. Introduction

Many are familiar with entering a mental “zone” characterized by intense concentration and self-absorption when engaging in compelling tasks (Csikszentmihalyi, 1975). In this state, our performance reaches its peak, but the state itself is temporary and may abruptly disappear after a period. This familiar state is known as *flow*, in which an individual is completely absorbed in an activity without reflective self-consciousness. Flow plays a pivotal role in enhancing task performance, promoting mental health, and fostering one's happiness in daily life (Csikszentmihalyi & LeFevre, 1989). However, studies focusing on the dynamics of flow reveal its unpredictability and discontinuity, often experienced as abrupt transitions into and out of the state (Ceja & Navarro, 2012). Capturing the swift fluctuations of flow holds the potential to unveil the mechanism behind its highly transient nature and effectively harness its dynamic properties.

Regrettably, current measurements of flow suffer from limitations in temporal resolution, hindering the comprehensive exploration of its temporal dynamics. Experience Sampling Methods (ESM) have been widely employed to investigate the dynamic patterns of flow, providing valuable insights into its temporal variations and uncovering phenomena such as chaos and hysteresis (Ceja & Navarro, 2009; 2012; Mackenzie, Hodge, & Boyes, 2011; Guastello, Johnson, & Rieke, 1999; Bricteux et al., 2017). Whereas, the limited temporal density

of sampling in ESM studies hampers their ability to capture the rapid fluctuations of flow occurring within minutes. This limitation is particularly problematic for tasks with short durations and rapidly changing contexts, such as aerial navigations, surgical operations, or sports like skiing and gliding. Real-time decoding of flow would set the initial reference for the closed-loop system to manipulate the flow state and to enhance performance. To achieve this goal, it is imperative to fill the gaps between ESM samplings during spare intervals. Therefore, this work aims to decode flow fluctuations with a high temporal resolution and explores the dynamics of flow state over time on a sub-minute timescale.

The subjective, complex, and multifaceted nature of flow poses several challenges when attempting to decode it on a fine timescale. Previous studies have emphasized that flow is composed of several mental components, including concentration, autotelic reward, cognitive control, etc. (Nakamura & Csikszentmihalyi, 2005; Huskey et al., 2018). Firstly, the subjectivity of flow necessitates the predominant use of self-reporting as the measurement approach, like the Flow Short Scale (FSS). The sampling sparsity of such measurements limits the timescale to the sub-hour level (Jackson, Martin, & Eklund, 2008). While some physiological tools offer the potential for higher temporal resolution in flow measurement, but flow state over a set period is typically calibrated based on self-reports or task challenge type, making it difficult to capture flow variations within minutes (Tozman et al., 2015; Tian et al., 2017; Berta et al., 2013; Katahira et al., 2018; Leroy & Cheron, 2020). Secondly, inducing the elusive flow experience under lab settings has proven challenging, requiring the manipulation of key factors such as optimal challenge, clarity of goals and feedback, and minimizing distractions (Moller, Meier, & Wall, 2010). Lastly, establishing and validating the models to describe flow is difficult due to its subjective and intricate nature, particularly regarding how the human behavior parameters are associated with flow (Bian et al., 2018).

Here, to break the limit of the timescale of flow measurements due to the sparsity of self-reporting, we propose a novel decoding framework that utilizes real-time task performance to track flow. The cornerstone of flow decoding lies in inducing it and monitoring its variations over time using explicit performance metrics, which necessitates a reliable task paradigm. The balance between challenge and skill has long been recognized as a core requirement for inducing flow, and previous research has employed computer games like Tetris (Harmat et al., 2015; Keller et al., 2011), mental arithmetic (Ulrich et al., 2014; Peifer et al., 2020) and simulated vehicle piloting tasks (Cowley et al., 2019; Palomäki et al., 2021; Hamari et al., 2016) to empirically induce flow. These experimental methodologies have advanced the study of flow from the observation on the people's daily life to the rigorous research under lab settings. However, in these approaches, the match between the challenge and skill is typically established by manually setting task difficulty to moderate, often overlooking individual differences in skill. Furthermore, to pursue high immersion and prevent boredom, these tasks lacked controlling over irrelevant factors and explicit performance indicators, limiting the quantitative tracking of flow. To address these limitations, we introduce a fine fingertip force control (F^3C) task that allows precise manipulation of task difficulty to align with an individual's skill. Fingertip force is measured in real-time for extracting metrics to represent performance variations. Given that the task comprises consecutive trials of 3-second duration, the performance metrics enable the decoding of flow on a second timescale.

To decode the flow variations via task performance metrics, it is crucial to establish the relationship between flow and performance. Previous studies have predominantly approached this by correlating self-reported flow experience with task performance of each subject (Harris et al., 2020; Engeser & Rheinberg, 2008), or proposing theories based on the components of flow (Baydas et al., 2015). These studies often treated the flow and task performance as static. Against this backdrop, we first expand upon the classical flow model by incorporating the variations of flow and performance, and then establish a force control model to elucidate how the flow intensity influences the task performance during the F^3C task. We validate the hypothesis that the task performance varies along with the flow intensity over time by extracting eight

performance metrics from the fingertip force sequence and comparing these metrics under distinct flow states. Subsequently, we attempt to decode flow by selecting the metrics with better predictive capability instead of using all the metrics to mitigate the risk of overfitting potentially caused by the sparsity of self-reporting. Finally, we investigate the dynamic characteristic underlying the fluctuations of flow on a sub-minute timescale. Our research unveils the presence of swift oscillations of flow variations within the intervals between self-reporting probes and offers a dynamic perspective on the relationship between flow experience and task performance.

2. Methods and theories

2.1. Participants

We recruited 32 right-handed adults from Beihang University [age 26.2 ± 4.4 y (mean \pm SD); eleven females]. Only subjects who reported normal vision or vision that was corrected to normal with contact lenses were included. We excluded volunteers who reported using medication that might influence the experiment. Participants were compensated with \$10 per hour. The experiment was approved by the Biological and Medical Ethics Committee of Beihang University (No. BM20230123) and was performed in accordance with the Declaration of Helsinki. Written informed consent was obtained from all participants before the experiment.

Two participants (both male) were excluded because their success rate was too high (exceeding 90%). We speculated they did not understand the pre-test task instructions on the skill measurement, resulting in the subsequent task that was too easy for their skill. They were excluded because the excessive successful rate meant the condition of flow occurrence, i.e., the challenge is as close to the skill as possible, cannot be ensured. Six participants (two females) were excluded for their self-reported results of flow probes. If the range of the self-reported flow intensity is too narrow, it is not sufficiently effective to be the ground truth for the decoding of flow variations. Hence, the participants whose range of self-reported flow intensity is less than 1 (for the seven-level Likert scale) were excluded. In the end, 24 participants [age 26.2 ± 4.4 y (mean \pm SD); nine females] were left for subsequent analyses, guaranteeing a match between challenge and skill and effectiveness of self-reporting, both of which are essential for flow decoding.

2.2. Flow induction: the F^3C task

According to the componential theory of flow (Csikszentmihalyi, 1975), the antecedents of the flow state are clear goals, unambiguous feedback, and a perfect match between skill and challenge. Herein, we designed a F^3C task to induce the flow experience: participants were instructed to precisely control their fingertip force within a specified target range by pressing the force transducer according to the visual presentation. The immersive virtual reality (VR) environment, provided by a head-mounted display device (Oculus Rift DK2), aimed to take over the sensory and minimize distractions, helping the participants concentrated on the task.

As illustrated in Fig.1 (b), we constructed a virtual disk and a cylinder with adjustable thickness within a virtual scenery using the Unity 3D engine. At the beginning of each trial, the virtual disk was positioned at the bottom of the user's view, while the virtual cylinder remained fixed at the center. As the participant pressed the force transducer (Arizon Technologies, mediated by the homemade sampling board, with the measuring error of 0.02%) using the right index finger, the virtual disk synchronously rose to a height proportional to the vertical pressing force. Participants were forbidden from pressing the transducer prior to the appearance of the virtual cylinder at the trial onset, ensuring that the pressing force sequence always starts at zero in each trial. Only by continuously maintaining the force F_t (denoted by the disk's height) in the target range ΔF (denoted by the thickness of cylinder) for a duration of over 500ms in a single trial with an upper time limit of 3s will

the participant succeed in the current trial. The green and red visual feedback denoting success and failure respectively would be presented after each trial. Participants were instructed to stabilize the force as much as possible during each trial and to strive for a higher number of successful trials. As depicted in Fig. 2 (b), the center of the grey cylinder corresponded to a vertical pressing force with the magnitude of 1N. The thickness of the cylinder, (i.e., the target range ΔF) served as an indicator of the task difficulty of the current trial. Smaller thickness corresponded to more challenging trials, requiring participants to exert greater effort to maintain the pressing force within the target range.

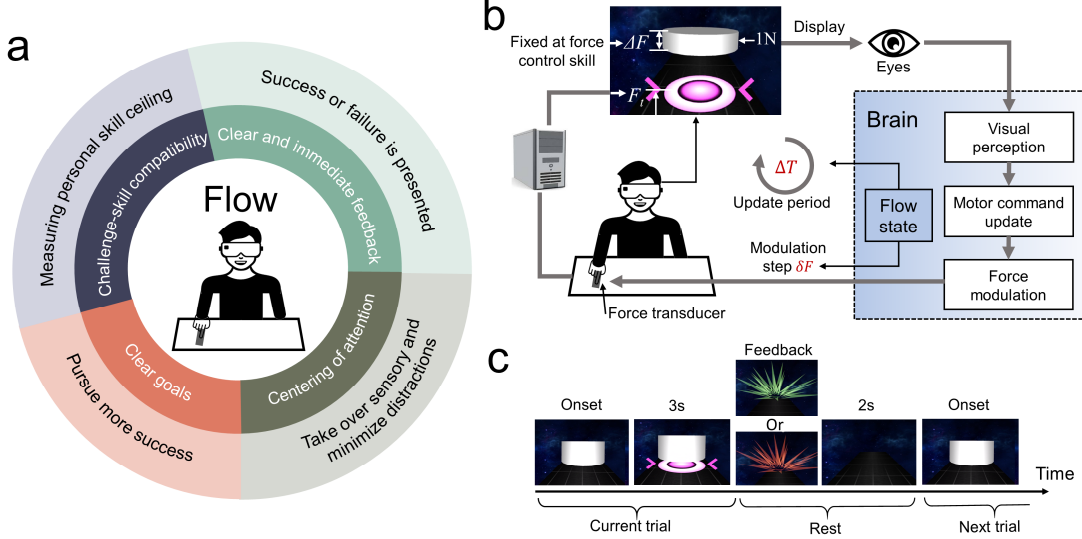


Fig. 1. The F³C task to induce the flow. (a) The design principles. The F³C task was designed to follow the main antecedents and components of flow. The inner circle represents the conditions of the flow and the outer circle represents the design elements of the task. (b) The details of the F³C task. During the task, the participant was instructed to press the force transducer using the right index finger to control the virtual disk (the height denotes the pressing force F_i) maintaining within the target range (denotes the force range ΔF) as much as possible. We assumed that the flow state influenced the force control performance mediated by affecting the updating period ΔT of the force control loop and minimum modulation step δF of fingertip force. (c) The procedure of the F³C task for a single trial, encompassing pressing duration of 3s and resting duration of 2s.

To account for individual variations in force control skill, we developed an adaptive procedure aimed at accurately measuring the skill ceiling for force control and precisely matching the task challenge to skill level. Drawing inspiration from the staircase approach used in psychophysiology (Jones & Tan, 2012) (Supplementary Note 1), our method involved adjusting the task difficulty based on participants' performance until a convergence point was reached. This convergence point was considered as the measured skill ceiling of fingertip force control. During the main experimental sessions, the task difficulty ΔF remained fixed at the measured skill, ensuring an optimal match between the challenge and skill.

2.3. Procedure

The experiment consisted of several components: a skill measurement session to assess the participant's force control skill, three sessions of the main experiment with a fixed task difficulty matching the measured skill, and a full-version Flow Short Scale (Jackson, Martin, & Eklund, 2008) to assess flow experience induced by the F³C task during the experiment at the end, as illustrated in Fig. 2.

Prior to the experiment, the participants were required to practice the F³C task till they adequately constructed the mapping relationship from fingertip motor command to the visual feedback provided in VR.

The skill measurement session encompassed 50 trials, following the adaptive procedure (Supplementary Note 1). Each main session comprised 100 trials, with 3-minute intervals between adjacent sessions to allow the participants to rest. Thus, each participant performed the F³C task for a total of 300 trials. The force output data during each trial were recorded at a sampling frequency of 1kHz for subsequent analysis. Additionally, leveraging simplified FSS, twelve flow probes were interspersed throughout the three main sessions to inquire the participants' current flow state as the ground truth of the flow decoding (Supplementary Note 2).

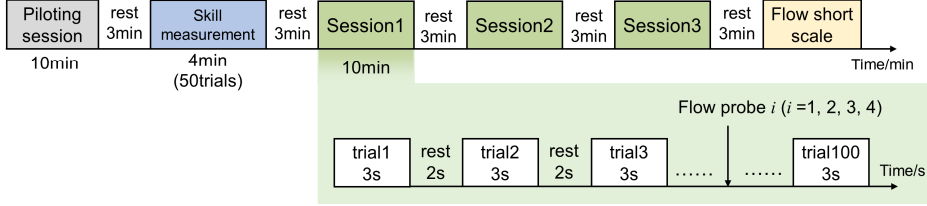


Fig. 2. The experimental procedure. Twelve flow probes were interspersed throughout the experiment to inquire the participants' current flow state.

2.4. Relationship between flow intensity and task performance

According to the classical channel model of flow (Csikszentmihalyi, 1990), the user would enter a flow state only when challenge and skill were in equilibrium (Fig. 3 (a)). For a specific task, the flow state can be entered only if the difference between challenge (C) and the measured ceiling of the skill (\hat{S}) was small enough (i.e., $C \in \{C | |C - \hat{S}| < \varepsilon\}$, ε represented a small enough positive number). Under that condition, the user's mental state would fluctuate between the in-flow state and the out-flow state dominated by the dynamic nature of the flow. In previous study, the concept of flow intensity was proposed to distinguish the different degrees of the flow experience (Percival, Crous, & Schepers, 2003). We can say the flow intensity would variate over time when challenge matched skill, as depicted in Fig. 3 (b) and (c).

Herein, we hypothesized that the task performance was influenced by the flow variation, fluctuating between high and low in correspondence to the mental state of in-flow and out-flow respectively, as depicted in Fig. 3 (c). If the influence on task performance from the flow variations was validated, the performance can be leveraged to distinguish the different flow states and decode the synchronous flow intensity.

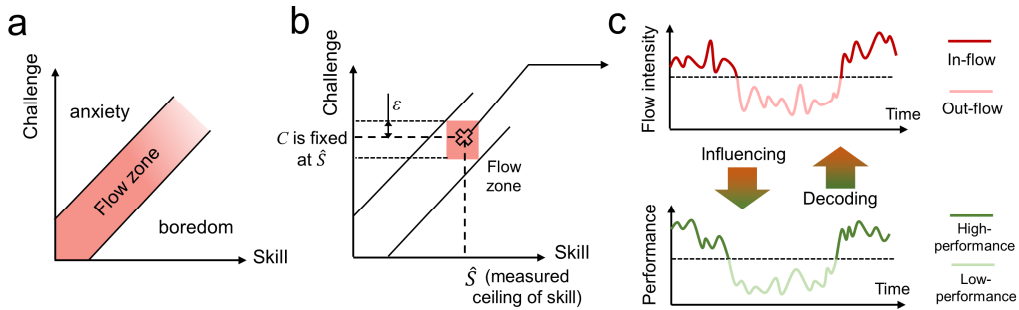


Fig. 3. Assumptions underlying the relationship between flow intensity and task performance. (a) The classical channel model of flow, describes that the balance between challenge and skill could induce flow experience. (b) For a specific task, the flow zone can be entered only if the difference between the challenge and the measured skill ceiling is small enough. Under that condition, the flow intensity of the user would fluctuate over time. (c) The task performance would be influenced by the flow fluctuation and the flow intensity variation could be decoded by the task performance over time.

2.5. Force control process and performance metrics

According to the section 2.4, we assumed that the task performance would be influenced by the flow intensity variations over time. In the context of the F³C task, this can be theoretically interpreted through the lens of the closed-loop force control process. During the task, participants' current fingertip force was translated into the height of the disk, and the discrepancy between the disk and cylinder served as the reference to make decision to alter the fingertip force. Then, the force was adjusted based on the motor command. It is believed that being in a flow state can expedite this force control loop, consequently influencing task performance. Our hypothesis posited that the flow intensity affected force output behavior, mediated by two critical parameters in the force control process: the updating period ΔT of the loop and the minimum modulation step of force δF , as depicted in Fig. 1 (b). As flow intensity increases, the force control loop would be facilitated to work, leading to a decrease in ΔT and δF . While the task performance would varied along with the decreasing of ΔT and δF .

To explicitly characterize the task performance of each trial, we defined eight metrics from the fingertip force output sequence, as follows and demonstrated in Fig. 4 (a):

- 1) *Reaction time*. The reaction time is defined as the duration from the trial onset to the timepoint when the force transducer detected the pressing force, which could be represented by t_1 in Fig. 4 (a).
- 2) *Arriving Time*. The arriving time is defined as the duration from beginning of the pressing to the timepoint when the fingertip force F_t reach the target range at the first time, i.e., t_2 in Fig. 4 (a).
- 3) *Completing time*. The completing time is defined as the duration from the trial onset to the timepoint the participant met the success condition before the trial is finished. The success condition is defined as a duration exceeding 500ms where pressing force was continuously in the target range (C.T. in Fig. 4 (a)).
- 4) *In-range time*. The in-range time indicates the cumulative duration of which the pressing force was in the target range before the trial is finished, which could be represented as the summation of t_3 , t_4 , and t_5 in Fig. 4 (a). Even though t_3 and t_5 are not to exceed 500ms.
- 5) *Force overshooting*. The force overshooting F_{OS} was defined as the peak of the fingertip force relative to the target force, as follows:

$$F_{OS} = |F_{\max} - F_T| / F_T \quad (1)$$

where F_{\max} denotes the peak force during the single trial and F_T denotes the target force (i.e., 1N).

- 6) *Average deviation*. The average deviation F_{AD} was defined as the averaged discrepancy between the current force and the target force at each sample, as follows:

$$F_{AD} = \sum_{i=1}^{N_s} |F_i - F_T| / N_s \quad (2)$$

where N_s represented the number of the force samples, and F_i denoted the force at the current sample.

- 7) *Average adjusting rate*. The average adjusting rate F_{ADR} was defined as the average change of the fingertip force at two adjacent samples, as follows:

$$F_{ADR} = \frac{\sum_{i=2}^{N_s} |F_i - F_{i-1}|}{(N_s - 1) \Delta t} \quad (3)$$

where F_i and F_{i-1} denoted the fingertip force at the current and the last sample respectively, Δt was the sampling period (i.e., 0.001s).

- 8) *Success rate*. For a single trial, the success or failure was marked as 1 and 0 respectively. Over several trials, the success rate was defined as the number of successful trials divided by the number of total trials.

These metrics were specifically designed to capture the influence of ΔT and δF and thereby distinguish different flow states. The influences on these metrics were supported by the simulation performed following the mathematical model for the fingertip force control process (Supplementary Note 3), as demonstrated in

Supplementary Fig. 1. The hypothesis stating that the task performance was influenced by the flow intensity variations can be tested by the self-reported flow intensity and the associated performance metrics of each flow probe during the experiment.

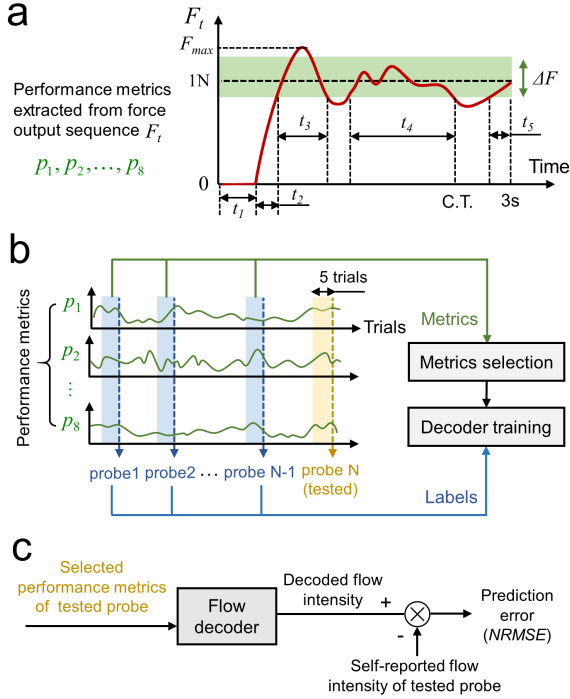


Fig. 4 (single column). Decoding framework of flow. (a) Extracting performance metrics from the output sequence within a single trial. The green band shows the target range of force control (i.e., ΔF). t_1 to t_4 denoted the temporal durations within the trial, being associated with the metrics. C.T. stands for the completing time. (b) Construction of the leave-one-out cross-validated flow decoder. For each participant, a flow probe (as an example, probe N) was left out as the tested probe to be predicted. The remaining flow probes and associated performance metrics were utilized to train the decoder. (c) The trained decoder was used to predict the tested flow probe (probe N) based on its associated selected performance metrics.

2.6. Construction of the flow decoder

According to the section 2.4, the flow intensity could be decoded by the synchronous task performance. For the F³C task, the task performance was characterized by eight metrics. For simplicity, the flow decoder can be represented by the linear mapping between the predicted flow intensity \hat{I}_t and the synchronous performance metrics, as follows:

$$\hat{I}_t = \mathbf{T}^* \mathbf{P}_t + I_0^* \quad (4)$$

where \mathbf{P} was the performance metrics vector, \mathbf{T}^* and I_0^* were the coefficients, which were determined within the flow decoder training. To select the metrics with better predictive capability while mitigating the risk of overfitting, we set a maximum limit of the decoding-used metrics as four and conduct the metrics selection process to obtain the metrics vector \mathbf{P} , instead of using all the eight metrics.

Let $\mathbf{\Omega}$ represent the full set of metrics vectors, $\mathbf{P} = [p_{a1}, p_{a2}, \dots, p_{an}]^T \in \mathbf{\Omega}$, where p came from the eight performance metrics we defined (i.e., $1 \leq a_1 \leq a_n \leq 8$). Supposing n metrics were selected for decoding ($n \leq 4$), then $\mathbf{P} \in R^{n \times 1}$ and $\mathbf{T}^* = [t_1, t_2, \dots, t_n] \in R^{1 \times n}$. For specific participant, we picked out every \mathbf{P} within $\mathbf{\Omega}$ to train the

flow decoder, ultimately identifying the \mathbf{P} associated with the optimal decoding performance as the designated decoding metrics vector. This metric selection procedure effectively ensured the number of flow probes surpassing three times the number of decoding features for each subject. Additionally, this process facilitated an understanding of which metrics exhibited greater diagnostic potential within the flow decoding context.

The flow decoding performance was evaluated by the leave-one-out cross-validation, as illustrated in Fig. 4 (b). For twelve flow probes of each participant, one probe was left out as the tested probe to be predicted. The remaining probes and associated performance metrics were utilized to train the decoder. We calculated each metric from the force output sequence of the previous five trials relative to the insertion timepoint of each probe (the number of trials was accordance with the flow probe questions) and averaged them across five trials as this metric associated with that probe. The decoder training process was to calculate \mathbf{T}^* and I_0^* to optimize the fitting between the predicted and the self-reported flow intensity, as follows:

$$(\mathbf{T}^*, I_0^*) = \underset{\mathbf{T}, I_0}{\operatorname{argmin}} \sum_{k=1}^{N-1} \|I^{(k)} - \mathbf{T}\mathbf{P}^{(k)} - I_0\|_2 \quad (5)$$

where N denoted the number of all flow probes (i.e., twelve), $I^{(k)}$ and $\mathbf{P}^{(k)}$ denoted the self-reported flow intensity and performance metrics vector associated with the k -th flow probe, and $\mathbf{P} \in \mathbf{\Omega}$. Once calculate \mathbf{T}^* and I_0^* by solving the optimization, the prediction of the tested flow probe could be obtained using the Eq. (4), and this process was repeated twelve times. By iteratively searching each metrics vector \mathbf{P} , we are capable of identifying the most optimal combination of performance metrics to effectively decode the flow.

2.7. Assessments of the flow decoder

The prediction error of flow decoding was determined by the discrepancy between the self-reported flow intensity of the tested probes and their prediction in each validation loop, as illustrated in Fig. 4 (c). We utilized the normalized root mean square error (*NRMSE*), a widely accepted index to represent prediction error. It was defined as:

$$NRMSE = \sqrt{\frac{\sum_{j=1}^N (\hat{I}^{(j)} - I^{(j)})^2}{\sum_{j=1}^N (I^{(j)})^2}} \quad (6)$$

where $I^{(j)}$ and $\hat{I}^{(j)}$ denoted the self-reported flow intensity and the prediction result of the j -th probe respectively. The smaller *NRMSE* represented the higher decoding accuracy. The correlation between self-reported and predicted flow intensities of the twelve probes can be used to assess the decoding performance.

Besides the correlation analysis, two statistical tests were employed to assess the flow decoder. (i) In the random-test, for each participant, we generated 1,000 sets of random sequences for each participant using the numbers drawn from the same range as self-reported flow intensity and place these at each probe. Cross-validated decoding was then performed repeatedly, using the same performance metrics, for each set of random flow labels. Consequently, we obtained a distribution of 1,000 cross-validated prediction errors following Eq. (6) for each subject. The random-test P -value was defined as the probability of obtaining lower cross-validated prediction error with random flow labels compared to true self-reported flow labels. (ii) In the permutation-test, we randomly permuted the time indices of the flow probes 1,000 times for each participant and repeated the procedure in the random-test to obtain the permuted-test P -values. The random-test was considered the primary criterion for determining significance, while the permuted-test was conducted to demonstrate the robustness of the decoder (Sani et al., 2018).

2.8. Statistics

The two-tailed independent samples *t*-tests were conducted on the comparison of the eight performance metrics associated with the in-flow and out-flow probes. The two-tailed paired samples *t*-tests were conducted to compare the prediction error among flow decoding, random-test, and permuted-test, as well as to compare the prediction error among the decoding of flow, fluency, and absorption. The statistical significance of flow decoding, both at the individual and population level was assessed by the random-test and permuted-test. The power spectral density (PSD) analysis, aiming to quantify the timescale of the fluctuation of the decoded flow intensity time series, was conducted by the Welch approach, which was implemented by the function *pwelch* in MATLAB. All the statistics were implemented using the SPSS (version 25.0) and MATLAB (version 2018b) and demonstrated after corrected with false discovery rate using the Benjamini–Hochberg approach.

3. Results

3.1. Flow induction

Following the experimental procedure, the skill ceiling of fingertip force control (represented by target force range ΔF) of each participant was measured before the three main sessions. The average measured skill across all participants was $0.040 \pm 0.013\text{N}$ (mean \pm SD). The success rates of each experimental session were demonstrated in Fig. 5 (a), in line with our hypothesis that the probability of success would be 0.5 when task difficulty matched the personal force control skill (Supplementary Note 1). This successful matching of task difficulty and personal skill ensured the prerequisite conditions for inducing the flow experience. Moreover, the full-version FSS was employed to assess the subjective flow experience during the experiment. The average score of FSS across all participants was 5.48 ± 0.71 (mean \pm SD, averaging ten questions within the scale) for seven-level Likert scale, affirming that the F^3C task effectively elicited the flow experience.

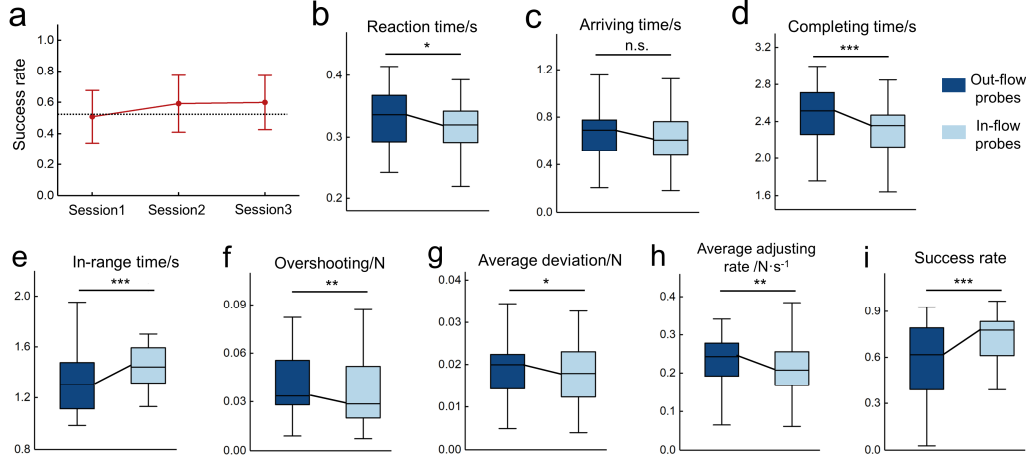


Fig. 5. The behavioral measures during the experiment. (a) The success rate during the three main experimental sessions. The error bars denote the standard deviation across subjects and the dot line denotes the success rate of 0.5. (b) to (i) demonstrate the eight performance metrics extracted from the force output sequence associated with the in-flow and out-flow probes across participants, compared by paired *t*-tests ($N=24$). Hinges of boxplots represent the first and third quartile and whiskers span from the smallest to the largest value of the data. * $P<0.05$, ** $P<0.01$, *** $P<0.001$, and n.s. stands for no significance.

3.2. Performance metrics

The eight performance metrics were used to substantiate the relationship between the task performance and flow intensity. For each participant, the median value of the self-reported flow intensities of all probes served as the criteria to categorize the probes into in-flow and out-flow probes. As demonstrated in Fig. 5 (b) to (i), the eight metrics associated with the in-flow and out-flow probes were compared by the paired t -tests ($N=24$). The results demonstrated that, except for the arriving time, the seven performance metrics associated with the out-flow probes exhibited significant differences in comparison to those associated with the in-flow probes (Supplementary Table 1). The trend of each metric's difference between in-flow and out-flow probes was the same as their simulation results (Supplementary Fig.1).

We further computed the correlation between the self-reported flow intensity and the associated performance metrics across all probes and subjects, yielding a total of 288 samples. Prior to analysis, z-standardization was applied to normalize the flow intensities and metrics for each subject. The corresponding t -tests were also conducted ($N=288$). The results demonstrated that all the eight metrics significantly correlated with the self-reported flow intensity (Supplementary Table 1). These findings suggest a notable capability of the task performance, as measured by the eight metrics, to differentiate distinct states of flow, taking the self-reported flow intensity as the ground truth, thus opening avenues for utilizing these performance metrics to decode variations in flow intensity during experimental sessions.

3.3. Flow decoding results

The eight performance metrics were selected to decode the self-reported flow intensity following the Eq. (4) and (5). For each participant, the flow decoder underwent training, followed by leave-one-out cross-validation, and subsequent statistical testing to assess the efficacy of flow decoding. Cross-validated prediction of the flow intensities of all the probes and all the subjects were depicted against the self-reported flow intensities in the Fig. 6 (a). The correlation analysis indicated a notably strong and significant correlation between the predicted values and the self-reported flow intensities ($R=0.81$, $P=1.54\times10^{-70}$), suggesting the flow decoder we trained by the performance metrics was highly predictive of the flow probes. At the individual level, Supplementary Fig. 1 exhibited the self-reported and predicted flow intensities of the twelve probes for each participant. The prediction error (measured by $NRMSE$) of flow and the Pearson's r of the correlation between self-reported and predicted flow intensities of twelve probes of each participant were documented in Supplementary Table 1. The results unveiled a significant correlation for 20 participants, emphasizing the precision of the flow decoding process at the individual level.

For various subject, different performance metrics were selected to decode flow through the metrics selection process. We calculated the relative decoding contribution of the selected metrics for each participant, as detailed in Supplementary Table 2. The summation of the relative decoding contribution attributed to each metric across all the participants was illustrated in Fig. 6 (b). Notably, while the average adjustment rate emerged as the most frequently utilized metric, it was the success rate that yielded the most cumulative contribution to the decoding. Conversely, both reaction time and completion time exhibited relatively modest contributions among the eight metrics.

The P -value and the probability density distribution of the random-test and the permuted-test for each participant were showcased in Supplementary Table 1, Fig. 2 and Fig. 3. The results demonstrated that we were capable of decoding the flow intensity by their performance metrics significantly (all the participants passed the random-test and permuted-test, taking $P<0.05$ as the passing criterion). As illustrated in Fig. 6 (c), the averaged prediction error (measured by $NRMSE$) of the true flow decoder across participants was both significantly less than that of random-test or permuted-test (true decoder vs. random-test: $t_{24}=-7.47$,

$P=1.37\times 10^{-7}$, Cohen's $d=1.52$; true decoder vs. permuted-test: $t_{24}=-7.01$, $P=3.79\times 10^{-7}$, Cohen's $d=1.43$; compared by paired t -tests). There was no significant difference between the averaged prediction error of random-test and permuted-test ($t_{24}=-1.792$, $P=0.086$, Cohen's $d=0.37$; compared by paired t -test). These results suggested that the decoding framework we proposed can effectively predict the flow intensity of each flow probe.

The flow intensity was self-reported through the two dimensions of fluency and absorption in the FSS. In this study, we kept these two dimensions when simplifying the FSS to design the flow probe (Supplementary Note 2). We repeated the flow decoding process to decode the fluency and absorption during the task using the same force output data and performance metrics, taking the subjective responses to the questions belonging to these two dimensions of each flow probe as the ground truth respectively. As listed in Supplementary Table 1 and demonstrated in Fig. 6 (d), the decoding accuracy reduced when the two dimensions were separated (flow intensity vs. fluency: $t_{24}=-2.88$, $P=0.008$, Cohen's $d=0.59$; flow intensity vs. absorption: $t_{24}=-2.81$, $P=0.01$, Cohen's $d=0.57$; fluency vs. absorption: $t_{24}=-1.57$, $P=0.13$, Cohen's $d=0.32$; compared by paired t -tests).

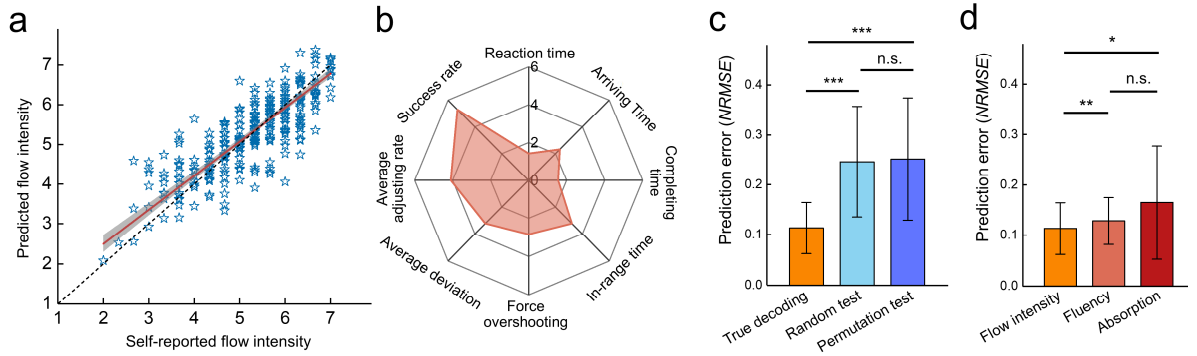


Fig. 6. Decoding flow intensity by associated performance metrics. (a) The correlation between the self-reported and predicted flow intensities of all the probes and all the participants. Each blue star depicts a flow probe and the black dot line denotes the ideal prediction. The red line represents the least squares fit, with grey shading showing the 95% CI. (b) The summation of the relative decoding contribution attributed to each metric across all the participants. (c) The averaged prediction error (measured by *NRMSE*) of true flow decoding, random-test and permuted-test across participants respectively, compared by paired t -tests ($N=24$). (d) Prediction errors (measured by *NRMSE*) for decoding flow intensity, fluency, and absorption, compared by paired t -tests ($N=24$). Fluency and absorption are two dimensions in the FSS and flow intensity is the combination of them. * $P<0.05$, ** $P<0.01$, *** $P<0.001$, and n.s. stands for no significance. The error bars denote the standard deviation across subjects.

3.4. Dynamics of decoded flow

Based on the evaluation of flow decoding, we were able to obtain the time series of flow intensities during the experiment from the performance metrics of each trial, using the trained flow decoder with the selected decoding-used performance metrics for each subject. An illustrative example was presented in Fig. 7 (a), where the decoded flow intensity fluctuated over time but aligned precisely with the self-reporting probes (indicated by the red stars). These findings highlighted that decoding flow using performance metrics enabled us to uncover the flow variations over time, particularly in the intervals between self-reporting points. This demonstrated our ability to overcome the temporal resolution limitations caused by the sparse placement of flow probes, allowing us to investigate the dynamics of flow on a sub-minute timescale.

Then the PSD analysis was conducted to quantify the timescale of the fluctuation of the decoded flow intensity. The PSD provided insights into the relative prominence of different timescales, which were defined as the inverse of frequency, within the decoded flow intensity time series. As demonstrated in Fig. 7 (b), the

results revealed that more than 70% of the power of flow intensity variations occurs at the timescales of 19.57 ± 2.71 s (mean \pm SD) and faster than that across participants. The results demonstrated that the sub-minute timescale oscillations predominantly contributed to the flow intensity variations. These fluctuations of flow become apparent in the intervals between self-reporting points, highlighting the dynamic nature that would have been overlooked without decoding flow using real-time performance metrics.

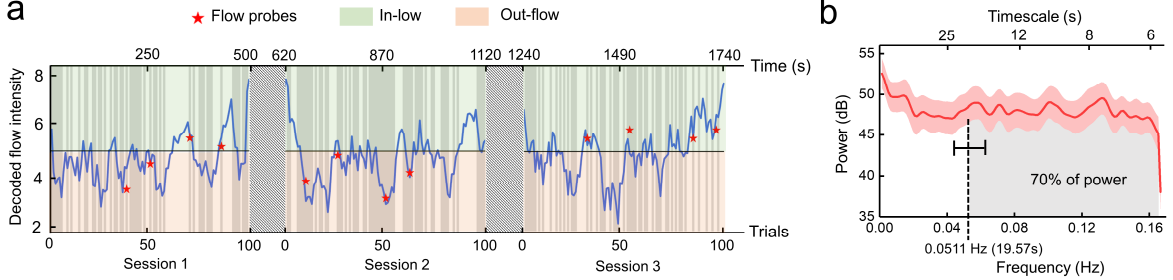


Fig. 7. The dynamics of the fluctuation of decoded flow intensity in the time and frequency domain. (a) The time series of the decoded flow intensity (taking example of subject #21). The two stripe bands represent the interval between consecutive experimental sessions. The vertical semi-transparent grey bands denote the failed trials (average success rate is 47.3%). The median of the self-reported flow intensities of the twelve probes served as the criteria to distinguish in-flow an out-flow states (i.e., the horizontal black line). (b) Estimated PSD of the decoded flow intensity time series. The vertical axis (dB units) is ten times proportional to the log of PSD in original units. The red line depicts the distribution of power on the frequency band from 0 to 0.167Hz (half of the sampling frequency of flow intensity time series 0.333Hz, i.e., inverse of the period of a single trial). The red shadow denotes the standard error of means across participants. Area under the curve over a certain set of frequencies is proportional to how prominent the decoded flow intensity variations are at those frequency band. The horizontal error bar represents the standard deviation of the lower bound of the frequency band in which the 70% of the power occurs across participants.

4. Discussion

In this work, the flow variations were decoded from task performance on a sub-minute timescale during the F³C task, supported by several empirical findings.

First, we proposed a F³C task to induce flow, and extracted eight metrics from the fingertip force sequence to represent task performance. Second, we find significant differences in eight performance metrics between in-flow and out-flow probes, providing evidence for our assumption that task performance could distinguish different flow states. These findings implied that the ambiguity of the relationship between flow and performance may due to the lacking of explicit behavioral indicators to track flow. Third, our findings confirm that flow intensity can be accurately predicted using selected performance metrics. Compared with the flow decoding via physiological or neural data (Rissler et al., 2018; Berta et al., 2013), we can not only decode flow on a fine timescale, but also consider the flow state as a continuous value, not just a state between in-flow and out-flow or among anxiety, flow, and boredom.

Inducing flow. The concept of flow is proposed based on the interviews and observation of the large populations with numerous professions, such as artists and athletes. In the last two decades, more and more experimental studies about flow were conducted in lab settings to investigate flow experience; in many of these studies, computer games were used to induce flow. The difficulty in most computer games, such as falling velocity in Tetris, could be adjusted among several levels, and moderate levels were most commonly chosen as a means of matching average participant skill level (Harmat et al., 2015; Keller et al., 2011; Chen & Sun, 2016). The insufficient quantification of challenge and skill for these game-based flow induction tasks makes it difficult to achieve customized matching between challenge and skill across different participants.

Flow research began with interviews about daily life experiences before transitioning to self-reporting in

ESM methods and eventually to accurate measurements in experimental studies; this demonstrates a trend towards increased explicitness of operational definition and parameterization of challenge and skill. For the F³C task, the challenge could be explicitly represented by the tolerance range of fingertip force control, which can be continuously altered to match the measured skill ceiling. Only under the personally matched challenge, can the human fingertip force control loop be sufficiently activated; this will make the user immersed in the task at hand, merge the action and awareness, and induce the flow experience.

Relationship between flow and motor performance. Previous literature has proposed several hypotheses and models discussing the relationship between flow and performance (Palomäki et al., 2021; Baydas et al., 2015). Since flow is composed of multiple mental components, it is believed that these components mediate the impact of flow on performance, including attention, motivation, motor automaticity, intrinsic rewards, etc. Because the task we used is more concerned with the effect of flow intensity on force control behavior on a sub-minute timescale, this implies that attention plays a more important mediating role (Weber et al., 2009). Attention has been verified to have second-level fluctuations, and its impact on task performance variation is explicit (Esterman et al., 2013; Jin et al., 2019; Rinne et al., 2018). Behavioral indicators such as reaction time have also been used to characterize and predict attention, inspiring us to decode flow state. However, the mediating role of attention in the F³C task needs to be further verified.

It is worth mentioning that the decoding accuracy reduced when we substitute the ground truth from the flow intensity into its two dimensions in FSS, performance fluency and mental absorption, as demonstrated in Fig. 6 (d). These results revealed, to an extent, that flow experience cannot be defined simply as attention or motor automaticity. Rather, flow is a complex and nuanced composition of multiple mental components.

The flow dynamics. Based on the classical channel model of flow, a series of mathematical models that quantitatively describe the impact of challenge and skill balance on flow were raised (Moneta & Csikszentmihalyi, 1996; 1999). These models were initially linear and static. However, the swift transition of flow imply that it is essential to investigate its dynamic characteristics. Researches revealed that the intrinsic nonlinear characteristics such as bifurcation points determine that the flow state will fluctuate indefinitely when challenge and skill are balanced (Mackenzie, Hodge, & Boyes, 2011; Guastello, Johnson, & Rieke, 1999). Hence, we proposed that the fluctuation of flow could be decoded at high temporal resolution using task performance.

Previous work related to flow dynamics proposed the Cusp catastrophe model, as well as dynamic properties such as hysteresis and phase transition (Ceja & Navarro, 2012). The data used for fitting these models usually were derived from the ESM, which limited the development of flow dynamics research. First, the ESM has deficits in measurement accuracy and controlling over irrelevant variables when doing various activities in daily life (Csikszentmihalyi & Larson, 2014). Second, the sparsity of ESM sampling limits the timescale of flow dynamics research. Against this backdrop, the methodology of this work is of great significance for exploring the flow dynamics on a finer timescale and under lab settings.

5. Conclusion

Based on the flow-inducing F³C task, our study showcases the ability to decode flow variations through performance metrics on a sub-minute timescale. This breakthrough overcomes the temporal limitations of the commonly used self-reporting approaches, like ESM. Our work not only expands the methodological possibilities for investigating flow dynamics with higher temporal resolution but also lays the foundation for future development of closed-loop systems capable of monitoring and regulating flow in the real-world dynamic context, like aerial navigations, benefiting a wider range of individuals.

References

- Baydas, O., Karakus, T., Topu, F. B., Yilmaz, R., Ozturk, M. E., & Goktas, Y. (2015). Retention and flow under guided and unguided learning experience in 3D virtual worlds. *Computers in Human Behavior*, 44, 96–102. <https://doi.org/10.1016/j.chb.2014.11.041>
- Berta, R., Bellotti, F., De Gloria, A., Pranantha, D., & Schatten, C. (2013). Electroencephalogram and Physiological Signal Analysis for Assessing Flow in Games. *IEEE Transactions on Computational Intelligence and AI in Games*, 5(2), 164–175. <https://doi.org/10.1109/TCIAIG.2013.2260340>
- Bian, Y., Yang, C., Zhou, C., Liu, J., Gai, W., Meng, X., Tian, F., & Shen, C. (2018). Exploring the Weak Association between Flow Experience and Performance in Virtual Environments. *Proceedings of the 2018 CHI Conference on Human Factors in Computing Systems*, 1–12. <https://doi.org/10.1145/3173574.3173975>
- Bricteux, C., Navarro, J., Ceja, L., & Fuerst, G. (2017). Interest as a moderator in the relationship between challenge/skills balance and flow at work: An analysis at within-individual level. *Journal of Happiness Studies*, 18(3), 861–880.
- Ceja, L., & Navarro, J. (2009). Dynamics of Flow: A Nonlinear Perspective. *Journal of Happiness Studies*, 10(6), 665–684. <https://doi.org/10.1007/s10902-008-9113-6>
- Ceja, L., & Navarro, J. (2012). ‘Suddenly I get into the zone’: Examining discontinuities and nonlinear changes in flow experiences at work. *Human Relations*, 65(9), 1101–1127. <https://doi.org/10.1177/0018726712447116>
- Chen, L.-X., & Sun, C.-T. (2016). Self-regulation influence on game play flow state. *Computers in Human Behavior*, 54, 341–350. <https://doi.org/10.1016/j.chb.2015.08.020>
- Cowley, B. U., Palomäki, J., Tammi, T., Frantsi, R., Inkilä, V.-P., Lehtonen, N., Pölönen, P., Vepsäläinen, J., & Lappi, O. (2019). Flow experiences during visuomotor skill acquisition reflect deviation from a power-law learning curve, but not overall level of skill. *Frontiers in Psychology*, 10, 1126. <https://doi.org/10.3389/fpsyg.2019.01126>
- Csikszentmihalyi, M. (1975). Beyond boredom and anxiety. San Francisco: Jossey-Bass.
- Csikszentmihalyi, M., & Larson, R. (2014). Validity and reliability of the experience-sampling method. In *Flow and the foundations of positive psychology* (pp. 35–54). Springer, Dordrecht.
- Csikszentmihalyi, M., & LeFevre, J. (1989). Optimal experience in work and leisure. *Journal of Personality and Social Psychology*, 56, 815–822. doi:10.1037/0022-3514.56.5.815.
- Engeser, S., & Rheinberg, F. (2008). Flow, performance and moderators of challenge-skill balance. *Motivation and Emotion*, 32(3), 158–172. <https://doi.org/10.1007/s11031-008-9102-4>
- Esterman, M., Noonan, S. K., Rosenberg, M., & DeGutis, J. (2013). In the zone or zoning out? Tracking behavioral and neural fluctuations during sustained attention. *Cerebral cortex*, 23(11), 2712–2723.
- Guastello, S. J., Johnson, E. A., & Rieke, M. L. (1999). Nonlinear dynamics of motivational flow. *Nonlinear dynamics, psychology, and life sciences*, 3(3), 259–273.
- Hamari, J., Shernoff, D. J., Rowe, E., Coller, B., Asbell-Clarke, J., & Edwards, T. (2016). Challenging games help students learn: An empirical study on engagement, flow and immersion in game-based learning. *Computers in Human Behavior*, 54, 170–179. <https://doi.org/10.1016/j.chb.2015.07.045>
- Harmat, L., de Manzano, Ö., Theorell, T., Högman, L., Fischer, H., & Ullén, F. (2015). Physiological correlates of the flow experience during computer game playing. *International Journal of Psychophysiology*, 97(1), 1–7. <https://doi.org/10.1016/j.ijpsycho.2015.05.001>
- Harris, D., Allen, K., Vine, S. J., & Wilson, M. (2020). A systematic review and meta-analysis of the relationship between flow states and performance [Preprint]. PsyArXiv. <https://doi.org/10.31234/osf.io/qg852>
- Huskey, R., Craighead, B., Miller, M. B., & Weber, R. (2018). Does intrinsic reward motivate cognitive control? A naturalistic-fMRI study based on the synchronization theory of flow. *Cognitive, Affective, & Behavioral Neuroscience*, 18(5), 902–924. <https://doi.org/10.3758/s13415-018-0612-6>
- Jackson, S. A., Martin, A. J., & Eklund, R. C. (2008). Long and Short Measures of Flow: The Construct Validity of the FSS-2, DFS-2, and New Brief Counterparts. *Journal of Sport and Exercise Psychology*, 30(5), 561–587. <https://doi.org/10.1123/jsep.30.5.561>
- Jin, C. Y., Borst, J. P., & Van Vugt, M. K. (2019). Predicting task-general mind-wandering with EEG. *Cognitive, Affective, & Behavioral Neuroscience*, 19(4), 1059–1073.
- Jones, L. A., & Tan, H. Z. (2012). Application of psychophysical techniques to haptic research. *IEEE transactions on haptics*, 6(3), 268–284.
- Katahira, K., Yamazaki, Y., Yamaoka, C., Ozaki, H., Nakagawa, S., & Nagata, N. (2018). EEG Correlates of the Flow State: A Combination of Increased Frontal Theta and Moderate Frontocentral Alpha Rhythm in the Mental Arithmetic Task. *Frontiers in Psychology*, 9, 300. <https://doi.org/10.3389/fpsyg.2018.00300>
- Keller, J., Bless, H., Blomann, F., & Kleinböhl, D. (2011). Physiological aspects of flow experiences: Skills-demand-compatibility effects on heart rate variability and salivary cortisol. *Journal of Experimental Social Psychology*, 47(4), 849–852. <https://doi.org/10.1016/j.jesp.2011.02.004>
- Leroy, A., & Cheron, G. (2020). EEG dynamics and neural generators of psychological flow during one tightrope performance. *Scientific Reports*, 10(1), 12449. <https://doi.org/10.1038/s41598-020-69448-3>
- Mackenzie, S. H., Hodge, K., & Boyes, M. (2011). Expanding the flow model in adventure activities: A reversal theory perspective. *Journal of Leisure Research*, 43(4), 519–544.

- Moller, A. C., Meier, B. P., & Wall, R. D. (2010). Developing an Experimental Induction of Flow: Effortless Action in the Lab. In B. Bruya (Ed.), *Effortless Attention* (pp. 191–204). The MIT Press. <https://doi.org/10.7551/mitpress/9780262013840.003.0010>
- Moneta, G. B., & Csikszentmihalyi, M. (1996). The effect of perceived challenges and skills on the quality of subjective experience. *Journal of personality*, 64(2), 275–310.
- Moneta, G. B., & Csikszentmihalyi, M. (1999). Models of concentration in natural environments: A comparative approach based on streams of experiential data. *Social Behavior and Personality: an international journal*, 27(6), 603–637.
- Nakamura, J., & Csikszentmihalyi, M. (2005). The concept of flow. In C. R. Snyder & S. Lopez (Eds.), *Handbook of positive psychology* (pp. 89–105). New York: Oxford University Press.
- Palomäki, J., Tammi, T., Lehtonen, N., Seittenranta, N., Laakasuo, M., Abuhamdeh, S., Lappi, O., & Cowley, B. U. (2021). The link between flow and performance is moderated by task experience. *Computers in Human Behavior*, 124, 106891. <https://doi.org/10.1016/j.chb.2021.106891>
- Peifer, C., Schönfeld, P., Wolters, G., Aust, F., & Margraf, J. (2020). Well Done! Effects of Positive Feedback on Perceived Self-Efficacy, Flow and Performance in a Mental Arithmetic Task. *Frontiers in Psychology*, 11, 10. <https://doi.org/10.3389/fpsyg.2020.01008>
- Percival, G., Crous, F., & Schepers, J. M. (2003). Cognitive potential and job complexity as predictors of flow. *The Journal of Individual Psychology*, 29, 60–71. <https://doi.org/10.4102/sajip.v29i2.96>
- Rinne, P., Hassan, M., Fernandes, C., Han, E., Hennessy, E., Waldman, A., ... & Bentley, P. (2018). Motor dexterity and strength depend upon integrity of the attention-control system. *Proceedings of the National Academy of Sciences*, 115(3), E536–E545.
- Rissler, R., Nadj, M., Li, M. X., Knierim, M. T., & Maedche, A. (2018). Got Flow?: Using Machine Learning on Physiological Data to Classify Flow. *Extended Abstracts of the 2018 CHI Conference on Human Factors in Computing Systems*, 1–6. <https://doi.org/10.1145/3170427.3188480>
- Sani, O. G., Yang, Y., Lee, M. B., Dawes, H. E., Chang, E. F., & Shanechi, M. M. (2018). Mood variations decoded from multi-site intracranial human brain activity. *Nature biotechnology*, 36(10), 954–961.
- Tian, Y., Bian, Y., Han, P., Wang, P., Gao, F., & Chen, Y. (2017). Physiological Signal Analysis for Evaluating Flow during Playing of Computer Games of Varying Difficulty. *Frontiers in Psychology*, 8, 1121. <https://doi.org/10.3389/fpsyg.2017.01121>
- Tozman, T., Magdas, E. S., MacDougall, H. G., & Vollmeyer, R. (2015). Understanding the psychophysiology of flow: A driving simulator experiment to investigate the relationship between flow and heart rate variability. *Computers in Human Behavior*, 52, 408–418. <https://doi.org/10.1016/j.chb.2015.06.023>
- Ulrich, M., Keller, J., Hoenig, K., Waller, C., & Grön, G. (2014). Neural correlates of experimentally induced flow experiences. *NeuroImage*, 86, 194–202. <https://doi.org/10.1016/j.neuroimage.2013.08.019>
- Weber, R., Tamborini, R., Westcott-Baker, A., & Kantor, B. (2009). Theorizing Flow and Media Enjoyment as Cognitive Synchronization of Attentional and Reward Networks. *Communication Theory*, 19(4), 397–422. <https://doi.org/10.1111/j.1468-2885.2009.01352.x>

Supplementary Materials

Supplementary Note 1. Adaptive procedure for measuring the force control skill

To achieve a balance between challenge and skill in the F³C task and to induce flow, it was crucial to accurately measure the skill ceiling of fingertip force control. Drawing inspiration from the widely-used staircase method in psychophysiology for threshold measurement, we devised an adaptive procedure to measure the skill. The fundamental principle of this adaptive procedure was to adjust the task difficulty (represented by the target force range, ΔF) of the next trial based on the performance of the current trial. If the current trial proved too challenging for the subject, the subsequent trial would be made easier; if the current trial was too easy, the next trial would be more difficult. We assumed that as the task difficulty increased, the likelihood of success decreased, and a difficulty level was considered suitable for the subject when the probability of success reached 0.5. If the task difficulty adapted with the performance, it would be converged at the value, under that the possibility of success or failure would be both 0.5. The point of convergence was considered as the measured skill. This converging value was calculated by averaging the task difficulties corresponding to the last ten transition points, where the difficulty sequence reversed, as depicted in Supplementary Fig. 1.

The design of the adaptive procedure considered two key requirements. The first requirement aimed to achieve swift convergence of the task difficulty. This entailed implementing a relatively large adjustment step (i.e., $\Delta F_{i+1} - \Delta F_i$, i is the current trial) of difficulty when the task was deemed too easy. The objective was to expedite the convergence process. The second requirement focused on ensuring measurement accuracy. To achieve this, it was essential to minimize the convergence range of the task difficulty and employ a relatively small adjustment step when the difficulty approached the skill ceiling. The basic idea was to make the adjustment step of difficulty decrease along with the number of the current trial, as follows:

$$|\Delta F_{i+1} - \Delta F_i|^{(1)} = \frac{k_1}{i} \quad (S1)$$

where k_1 denoted the coefficient. The sign of $|\Delta F_{i+1} - \Delta F_i|$ would be negative or positive when the current trial was successful or unsuccessful.

Then the performance of the current trial was involved. For simplicity, the completing time of each trial was considered to represent the performance. The adjustment step could be represented as follows:

$$|\Delta F_{i+1} - \Delta F_i|^{(2)} = \frac{k_2}{t_{Com}} \quad (S2)$$

where the t_{Com} denoted the completing time of the current trial and k_2 denoted the coefficient. The sign of $|\Delta F_{i+1} - \Delta F_i|$ would be negative or positive when the current trial is successful or unsuccessful.

At last, in order to avoid the adjustment step being too large relative to the current difficulty, we set a limit of the adjustment step by the current difficulty, which could be represented as follows:

$$|\Delta F_{i+1} - \Delta F_i|^{(3)} = 0.5\Delta F_i \quad (S3)$$

Combine these factors, the adjustment step of difficulty was determined by the number, performance, and the difficulty of the current trial, which was derived as:

$$|\Delta F_{i+1} - \Delta F_i| = \min \left\{ \frac{k_1}{i}, \frac{k_2}{t_{Com}}, 0.5\Delta F_i \right\} \quad (S4)$$

The adjustment step was the minimum among Eq. (S1), (S2), and (S3). The sign of $|\Delta F_{i+1} - \Delta F_i|$ would be negative or positive when the current trial was successful or unsuccessful.

Supplementary Note 2. The implementation of flow probes

During the F³C task, it was essential to measure the self-reported flow intensity at different time as the ground truth. However, self-reporting can disrupt the continuity of the task and potentially interrupt the flow experience. Therefore, it was crucial to limit the number of self-reporting timepoints, also known as flow probes. A total of twelve flow probes were used, with four probes inserted in each session. The interval between two adjacent probes was set to a minimum of twelve trials to avoid excessive insertion of probes within a short time period. When a flow probe was inserted, participant would encounter a pop-up dialog box in the virtual scenery, inquiring about their current flow state.

Flow short scale (FSS) was a widely used tool for measuring flow, consisting of ten questions that can be categorized into two dimensions: the fluency of performance (six questions) and the absorption by activity (four questions). It employed a seven-level Likert scale to assess subjective flow experience. The average of the participants' responses to the ten questions served as the assessment result. To minimize the interruption, we carefully selected three questions from the FSS that still encompassed both dimensions. The selection was based on interviews conducted with participants from a preliminary study, wherein we inquired about their experimental experiences. The content of the flow probe was as follows:

Please choose the answer from one to seven based on your thoughts and feelings in the previous five or so trials. There are no right or wrong answers.

- 1) *My thoughts/activities run fluidly and smoothly.*
- 2) *I have no difficulty concentrating.*
- 3) *I do not notice time passing.*

One denotes not at all, four denotes partly, and seven denotes strongly agree.

Among the three selected questions, the first and second questions pertain to the dimension of fluency, while the third question related to the dimension of absorption by activity. The average of the participants' responses to these three questions served as the self-reported flow intensity for the current probe.

Supplementary Note 3. Mathematical model on fingertip force control process

We established the mathematical model to describe the closed-loop fingertip force control process (Fig. 1(b)) following the physiological fundamentals. During the task, the fingertip force modulation could be represented as follows:

$$F^{(t+\Delta T)} = F^{(t)} + \Delta F_M^{(t)} + w_F \quad (S5)$$

where $F^{(t+\Delta T)}$ and $F^{(t)}$ denoted the pressing force at the timepoint $t+\Delta T$ and t respectively. ΔT denoted the period of the force control loop and w_F denoted the force output noise. $\Delta F_M^{(t)}$ represented the modulated force, which was determined by the motor command $\Delta F_C^{(t)}$ and limited by the minimum modulation step of fingertip force δF , as follows:

$$\Delta F_M^{(t)} = \begin{cases} \left\lceil \frac{\Delta F_C^{(t)}}{\delta F} \right\rceil \delta F, & |\Delta F_C^{(t)}| > \delta F \\ \Delta F_C^{(t)}, & |\Delta F_C^{(t)}| \leq \delta F \end{cases} \quad (S6)$$

The motor command was generated after motor decision making, in which the participants make decisions about the fingertip force modulation based on the visual information. The motor command could be derived as follows:

$$\Delta F_C^{(t)} = k_F (H_0 - H^{(t)}) + w_C \quad (S7)$$

where $H^{(t)}$ and H_0 represented the current height and the target height observed by the subject. w_C denoted the error of the decision making and k_F is the coefficient. Eq. (S7) showed that the human update the motor command based on the bias between the current and the target height.

The current fingertip force was measured by the force transducer and transformed into the height of the virtual disk, which could be represented as follows:

$$H^{(t)} = k_H (F^{(t)} + w_M) + w_V \quad (S8)$$

where w_M and w_V respectively denoted the error of the fingertip force measurement and subject's visual observation. Coefficient k_H is the inverse of k_F . The force control model for the F³C task encompassed the Eq. (S5) to (S8), as depicted in Supplementary Fig. 2, where the ΔT and δF would be influenced by the flow intensity.

Based on this model, we simulated the closed-loop force control process and investigate how the performance metrics are influenced by ΔT and δF . The results showed that all the eight performance metrics were capable of indicating the influence of ΔT and δF (Supplementary Fig. 3).

Supplementary Table 1. The statisticcal results of the eight performance metrics.

Performance metric	Paired <i>t</i> -test (<i>N</i> =24)			Correlation (<i>N</i> =288)	
	<i>t</i> -value	<i>P</i> -value	Cohen's <i>d</i>	Pearson's <i>r</i>	<i>P</i> -value
Reaction time	-2.74	0.012*	0.56	-0.25	1.23×10^{-5} ***
Arriving time	-1.85	0.078	0.38	-0.12	0.044*
Completing time	-5.40	1.76×10^{-5} ***	1.10	-0.28	2.04×10^{-6} ***
In-range time	4.94	5.39×10^{-5} ***	1.01	0.30	2.53×10^{-7} ***
Force overshooting	-3.06	0.006**	0.62	-0.27	3.80×10^{-6} ***
Average deviation	-2.67	0.014*	0.54	-0.30	2.18×10^{-7} ***
Average adjusting rate	-3.12	0.005**	0.64	-0.24	4.16×10^{-5} ***
Success rate	6.24	2.3×10^{-6} ***	1.27	0.39	9.44×10^{-12} ***

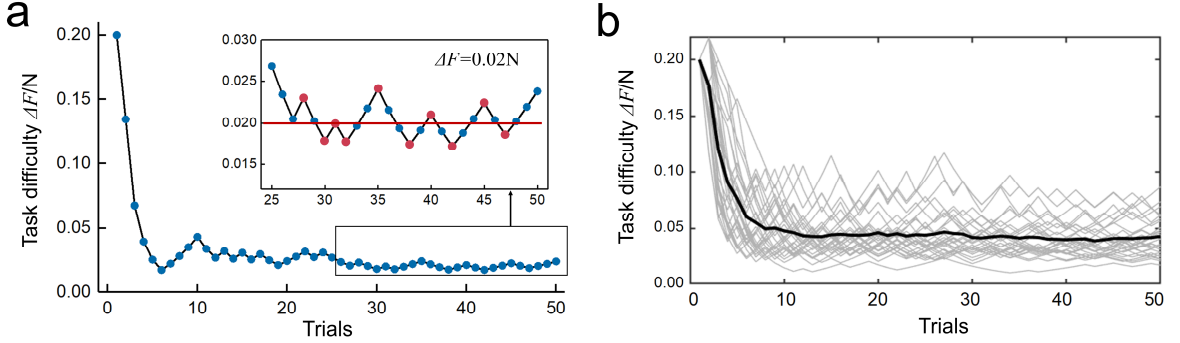
Note. * $P < 0.05$, ** $P < 0.01$, and *** $P < 0.001$. Each performance metric of in-flow probes and out-flow probes was compared by the paired *t*-tests (*N*=24). The Pearson correlations between the self-reported flow intensity and each associated performance metrics across all probes and subjects were conducted (*N*=288).

Supplementary Table 2. Flow decoding results for each subject.

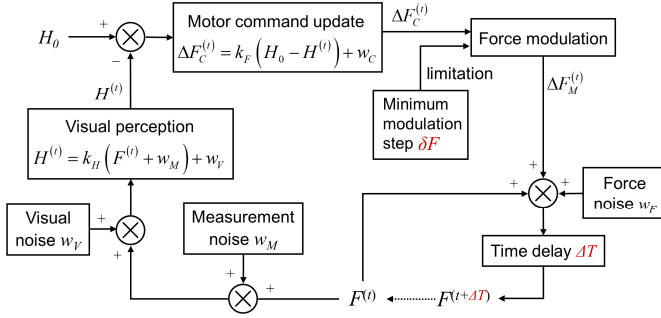
Subject	Flow intensity prediction error	Pearson's r (self-reported vs. decoded flow)	P -value of random-test	P -value of permuted -test	Fluency prediction error	Absorption prediction error
1	13.38%	0.57	0.007**	0.018*	19.05%	10.28%
2	7.30%	0.76**	0.003**	0.003**	8.41%	5.61%
3	13.05%	0.41	0.038*	0.033*	15.39%	19.46%
4	6.85%	0.76**	0.001**	0.001**	11.04%	14.62%
5	20.12%	0.74**	<0.001***	0.004**	22.89%	21.78%
6	7.38%	0.66*	0.001**	0.017*	7.20%	11.10%
7	4.25%	0.94***	<0.001***	<0.001***	12.56%	33.97%
8	21.71%	0.64*	0.007**	0.012*	12.90%	56.79%
9	15.43%	0.77**	0.002**	0.007**	16.93%	16.44%
10	20.34%	0.81**	<0.001***	0.001**	12.97%	18.96%
11	9.72%	0.59*	0.002**	0.002**	13.87%	4.41%
12	7.95%	0.81**	<0.001***	<0.001***	9.28%	8.68%
13	9.95%	0.67*	0.005**	0.003**	10.58%	11.65%
14	5.21%	0.73**	0.002**	0.001**	3.36%	16.19%
15	16.71%	0.52	0.016*	0.015*	17.30%	21.62%
16	6.42%	0.82**	<0.001***	<0.001***	7.64%	10.02%
17	13.59%	0.67*	<0.001***	<0.001***	15.86%	18.49%
18	10.70%	0.7*	<0.001***	0.001**	13.22%	9.23%
19	6.31%	0.93***	<0.001***	<0.001***	13.52%	16.73%
20	9.07%	0.87***	<0.001***	<0.001***	7.55%	12.51%
21	12.13%	0.67*	<0.001***	<0.001***	16.68%	24.13%
22	17.15%	0.43	0.007**	0.007**	16.83%	20.10%
23	13.34%	0.58*	0.004**	0.003**	16.27%	12.88%
24	4.23%	0.62*	0.001**	0.001**	6.48%	0.00%
Mean	11.34%	-----	-----	-----	12.82%	16.49%

Note. * $P<0.05$, ** $P<0.01$, and *** $P<0.001$. The prediction error for each participant is measured by the normalized root mean square error (*NRMSE*). The third column shows the Pearson's r of the correlation between the self-reported and the decoded flow intensities of twelve flow probes for each participant. The asterisks in the third column indicate the corresponding t -tests results.

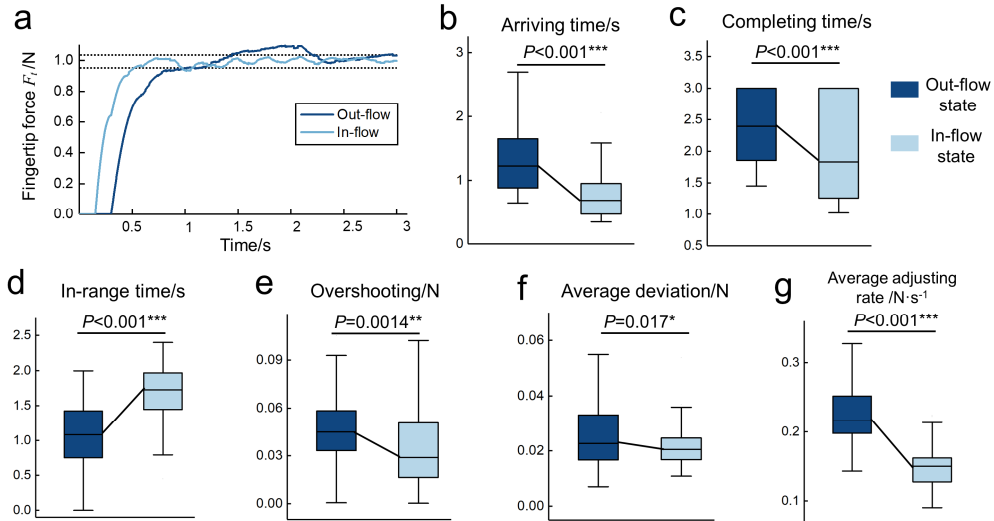
Supplementary Fig. 1. Personalized force control skill measurements. (a) Schematic of measurement approach, taking subject#24 as an instance. Each blue dot denotes the task difficulty (i.e., target force range, ΔF) in each trial during the measurement session (consisting of 50 trials). The red dots in subfigure represent the last ten transition points, where the task difficulty sequence reverse, and the red line indicates the measured skill by averaging the task difficulties corresponding to the transition points. (b) The task difficulty variate during the measurement session. The task difficulty shows the tendency of decreasing and converging. Each grey line denotes each participant and the bold black line denotes the average task difficulty variation across all participants.



Supplementary Fig. 2. The mathematical model describing the fingertip force control mechanism during the F³C task



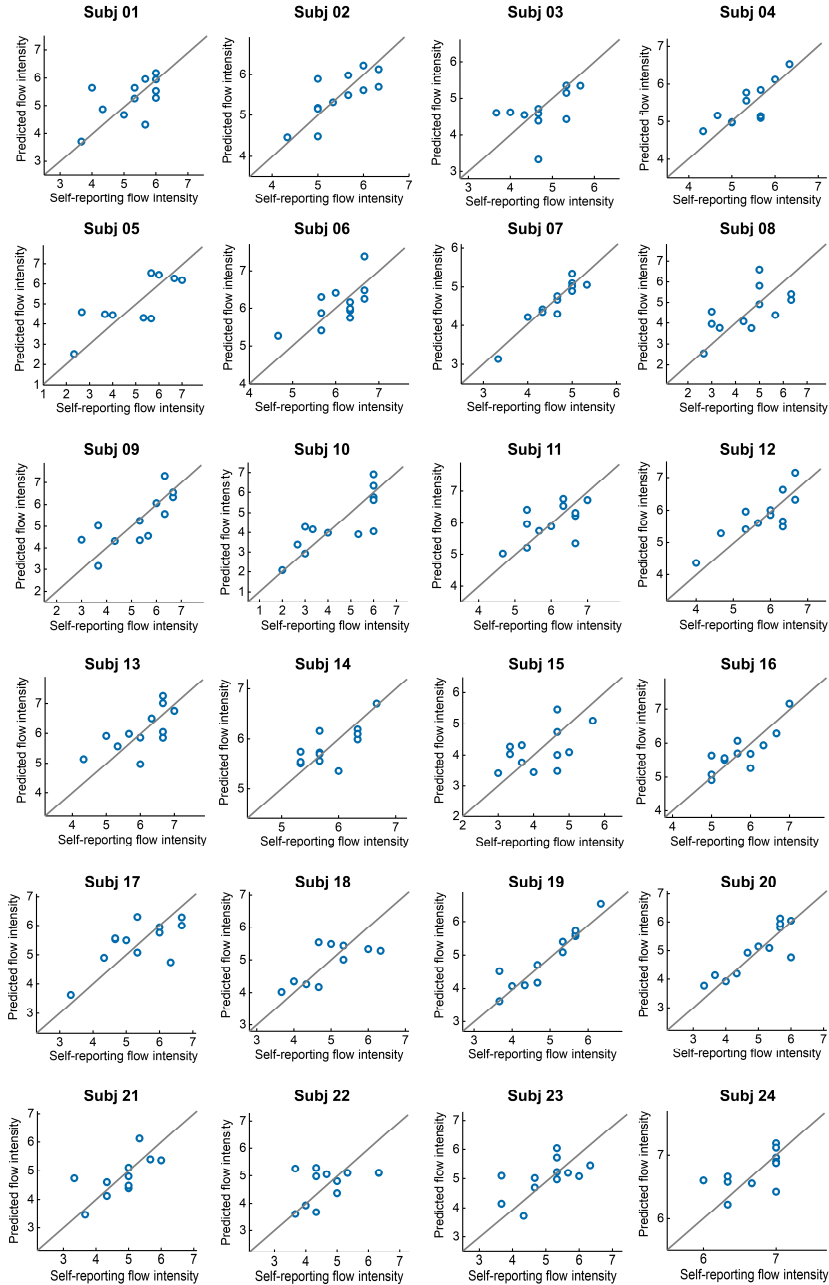
Supplementary Fig. 3. The simulation results of the force control model. (a) The example of simulated fingertip force sequence under in-flow and out-flow states. The dot lines denote the current target range of force control, $\Delta F=0.055\text{N}$. The simulation was implemented following the mathematical model of force control behavior (Supplementary Note 3), i.e., the Eq. (S5) to (S8). According to our hypothesis, the force control loop would be facilitated to work along with the increase of flow intensity, and ΔT and δF would decrease in the meantime. The manipulation of the two different flow state is conducted by altering the ΔT (in-flow: 0.15s vs. out-flow: 0.3s) and δF (in-flow: 0.015N vs. out-flow: 0.03N) in the mathematical model of force control process (Supplementary Note 3), without changing any other parameters in the model. (b) to (g) show the six performance metrics extracted from the simulated force output sequence under out-flow and in-flow states. The simulation and metrics calculation were conducted for 100 times, the same as the number of trials in a single session. The metric reaction time can be derived directly from the force control model (i.e., reaction time= ΔT). The metric success rate cannot be calculated for a single trial (the average success rate: in-flow is 0.61 and out-flow is 0.47), so the results of the remaining six metrics are demonstrated. The metrics under out-flow and in-flow states are compared by the two-tailed paired-samples t -tests ($N=100$). Hinges of boxplots represent the first and third quartile and whiskers span from the smallest to the largest value of the data. * $P<0.05$, ** $P<0.01$, and *** $P<0.001$.



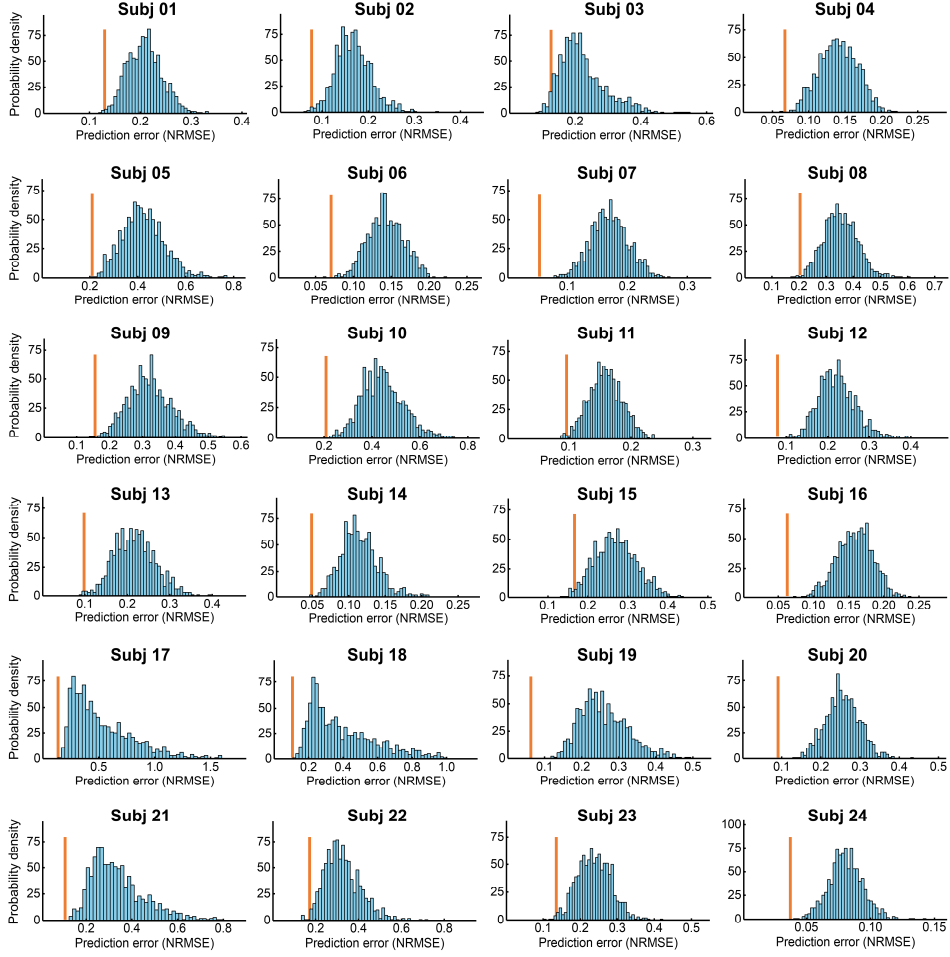
Supplementary Fig. 4. The selection and relative decoding contribution of decoding-used performance metrics for each subject. Note. In the Eq. (4), the coefficients t_1, t_2, \dots, t_n in vector \mathbf{T}^* are capable of measuring the decoding contributions of their corresponded metrics after the decoding-used metrics are z-standardized for each participant. The relative decoding contribution of a metric refers to the proportion of the absolute value of its corresponding coefficient t to the sum of the absolute values of all the coefficients within \mathbf{T} for a specific subject. Consequently, for each subject, the summation of the relative decoding contributions of all the decoding-used metrics amounts to 1. The null positions within the table indicate that the corresponding metrics are not selected for decoding.

Subject	Reaction time	Arriving time	Completing time	In-range time	Force overshooting	Average deviation	Average adjusting rate	Success rate
1	0.19		0.33	0.13	0.35			
2	0.45				0.35	0.20		
3			0.11	0.40	0.50			
4	0.17		0.25	0.28		0.30		
5								1.00
6	0.18		0.17	0.24		0.41		
7	0.20	0.30			0.29	0.21		
8					0.46	0.54		
9		0.28						0.72
10			0.39	0.61				
11	0.19	0.25		0.29				0.27
12	0.18		0.50			0.32		
13				0.29		0.45	0.26	
14		0.29	0.24	0.47				
15		0.32		0.49	0.19			
16		0.23		0.30		0.10	0.37	
17			0.11		0.38	0.52		
18								1.00
19	0.05		0.17		0.31		0.47	
20			0.17			0.30	0.52	
21		0.18			0.39	0.43		
22						0.32	0.68	
23			1.00					
24		0.29		0.56	0.15			
Sum	1.42	2.32	1.55	3.22	2.85	3.22	4.10	5.30
Using frequency	7	9	5	9	9	9	12	9

Supplementary Fig. 5. Cross-validated decoding performance of each participant. The prediction of flow intensity of each participant was obtained following the decoding framework, compared with the self-reporting flow intensity in each probe. Each blue dot represents a flow probe and the grey lines indicate the ideal prediction.



Supplementary Fig. 6. Probability density distribution of the prediction errors (measured by the normalized root mean square error, *NRMSE*) for 1,000 random sets of the flow intensity of each participant, compared with the true set of the flow intensity in each probe. The orange line denotes the prediction error in the decoding taking true set of the flow intensity in each probe.



Supplementary Fig. 7. Probability density distribution of the prediction errors (measured by the normalized root mean square error, *NRMSE*) for 1,000 permuted sets of the flow intensity of each participant, compared with the true set of the flow intensity in each probe. The orange line denotes the prediction error in the decoding taking true set of the flow intensity in each probe.

